J. Fluid Mech. (2013), *vol.* 726, R1, doi:10.1017/jfm.2013.239

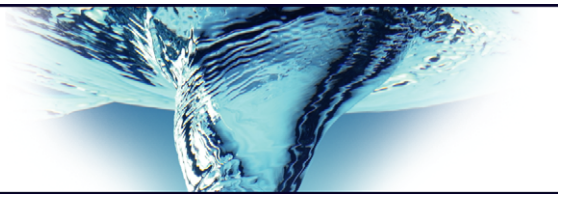

JFM RAPIDS
journals.cambridge.org/rapids

Circulation-based models for Boussinesq internal bores

Zachary Borden and Eckart Meiburg†

Department of Mechanical Engineering, University of California at Santa Barbara, Santa Barbara, CA 93106, USA

(Received 9 March 2013; revised 2 May 2013; accepted 7 May 2013;
first published online 30 May 2013)

Existing control-volume models for predicting the front velocity of internal bores enforce the conservation of mass and streamwise momentum, but not vertical momentum. Instead, they usually invoke an empirical assumption relating the up- and downstream energy fluxes to obtain an additional equation required for determining the pressure jump across a bore. The present investigation develops a control-volume model for internal bores on the basis of mass and momentum conservation alone, without the need for considering energy. This is accomplished by combining the streamwise and vertical momentum equations to obtain a vorticity relation that no longer involves pressure. Hence, this vorticity equation, in combination with the conservation of mass, is sufficient for evaluating the bore velocity. The energy loss across the bore can then be predicted by the streamwise energy equation and compared to the assumptions underlying earlier models. The flux of vorticity across the internal bore predicted by the new model is seen to be in close agreement with direct numerical simulation results. Any discrepancies with experimentally measured bore velocities are shown to be due to the effects of downstream mixing.

Key words: geophysical and geological flows, stratified flows, vortex dynamics

1. Introduction

Internal bores occur in a wide variety geophysical flows. In the atmosphere, they arise from the interaction of sea-breezes or thunderstorm outflows with inversion layers (Clarke, Smith & Reid 1981; Haase & Smith 1984; Wakimoto & Kingsmill 1995). In marine environments, they can be caused by the breaking of internal waves (Leichter *et al.* 1996), by tides interacting with seafloor topography (Morozov *et al.* 2002), or by gravity current flows past submarine obstacles (Gonzalez-Juez *et al.* 2010). Several analytical models have been proposed to relate the speed of propagation of a bore to

† Email address for correspondence: meiburg@engineering.ucsb.edu

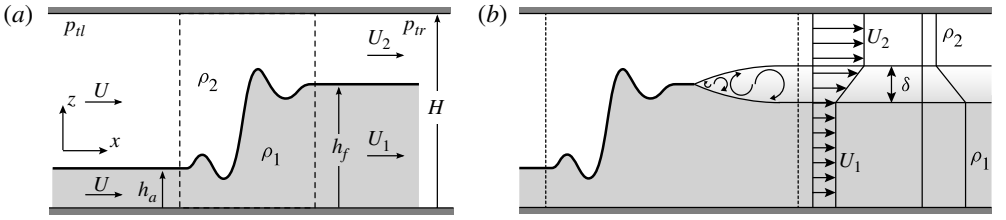

FIGURE 1. (*a*) Simplified geometry of an internal bore used by Wood & Simpson (1984), Klemp *et al.* (1997) and Borden *et al.* (2012). (*b*) The same simple geometry, but with a shear layer of finite thickness separating the upper and lower layers. The velocity and density vary linearly across the layer.

its size, but these models usually invoke an empirical assumption about the change in energy flux across the bore. On the other hand, computational investigations based on Navier–Stokes simulations are able to reproduce the dynamics of internal bores from mass and momentum considerations alone (Borden, Meiburg & Constantinescu 2012), which suggests the same should be possible for an analytical model.

In this investigation, we develop a closed-form analytical model for internal bores without the need for an energy assumption by considering the flux of vorticity across the front of a bore. We compare the new model with two-dimensional direct numerical simulation results, and show that any discrepancy between the predicted and actual front velocity of a bore can be explained by considering the effect of mixing at the downstream interface on the conservation of mass in each fluid layer.

2. Analytical models for Boussinesq internal bores

Existing models of two-layer internal bores, particularly those of Wood & Simpson (1984), Klemp, Rotunno & Skamarock (1997) and Borden *et al.* (2012), consider the flow sketched in figure 1(*a*) to derive an expression for the bore velocity U in terms of the geometrical parameters H, h_f and h_a. Following the approach of Rayleigh (1914) in his work on single-layer hydraulic jumps, each model makes the following assumptions: that the bore propagates at a steady velocity U, that the pressure field far up- and downstream of the front is hydrostatic, and that viscous effects are negligible. In a control volume around the front of the bore, each model enforces the conservation of mass within each layer, along with the conservation of overall streamwise momentum

$$U_1 h_f = U h_a, \tag{2.1}$$

$$U_2(H - h_f) = U(H - h_a), \tag{2.2}$$

$$\int_0^H (p_l + \rho U^2)\,\mathrm{d}z = \int_0^H (p_r + \rho u_r^2)\,\mathrm{d}z, \tag{2.3}$$

where u_r represents the local velocity far downstream of the front, and p_l and p_r indicate the hydrostatic pressure plus the pressure at the top of the channel (p_{tl} and p_{tr}) at streamwise locations far up- and downstream of the front.

It would seem that we have three equations available to solve for U, U_1 and U_2 in terms of the given values of H, h_f, h_a, ρ_1 and ρ_2. However, (2.3) introduces an additional unknown: the pressure jump across the front along the top wall of the channel, $p_{tl} - p_{tr}$. Therefore, unlike for single-layer hydraulic jumps, the

conservation equations for mass and streamwise momentum alone do not provide enough information for a closed-form solution. An additional equation is required.

Traditionally, this fourth equation has been obtained by making an assumption about the conservation of mechanical energy across the front of the bore. Wood & Simpson (1984) assumed that, similar to a single-layer hydraulic jump, no energy should be lost across the front of the bore in the light, upper-layer fluid. By equating the energy fluxes in and out of the control volume in the upper layer, they obtained the front velocity

$$u_{ws} = \left\{ \frac{R(1+R)(1-Rr)^2}{R^2 r - 3Rr + 2} \right\}^{1/2}, \tag{2.4}$$

where $R = h_f/h_a$, $r = h_a/H$ and $u = U/(g' h_a)^{1/2}$ is the non-dimensional front velocity (with $g' = g(1 - \rho_2/\rho_1)$ denoting the reduced gravity). We hereafter refer to this model as WS.

Later, Klemp *et al.* (1997) discovered that they obtained closer agreement with laboratory experiments of internal bores if they instead applied conservation of energy across the front of the bore in the heavy, lower-layer fluid. This produces the front velocity

$$u_{krs} = \left\{ \frac{R^2[2 - r(1+R)](1-Rr)}{R^2 r - 3Rr + R + 1} \right\}^{1/2}, \tag{2.5}$$

which we refer to as the KRS model.

Based on direct numerical simulations (DNS) of internal bores, Borden *et al.* (2012) show that within an internal bore mechanical energy is lost due to turbulent mixing in the interfacial shear layer, cf. figure 1(*b*). Furthermore, this turbulent mixing can result in a net energy transfer from the contracting to the expanding layer. By solving for the amount of energy lost in the mixing layer, the authors obtain a front velocity that is a function of the Reynolds and Schmidt numbers as well as R and r. Hereafter, we denote their front velocity as the BMC model.

2.1. *Circulation-based model*

Within this investigation, we pursue an alternative approach for deriving an expression for the bore velocity. As explained above, in the earlier models the need for invoking an energy argument arose from the fact that the streamwise momentum equation (2.3) introduced the pressure difference along the top wall as an additional unknown. Hence, if we were able to impose the conservation of momentum in a form that does not involve the pressure, the energy equation would no longer have to enter into our considerations. This can indeed be accomplished by focusing on the well-known vorticity formulation of the momentum conservation principle, which eliminates the pressure variable by taking a linear superposition of the streamwise and vertical momentum equations.

Consider the internal bore with the simple geometry and sharp interface in figure 1(*a*). Conservation of mass remains as stated in (2.1) and (2.2). But, instead of enforcing the conservation of streamwise momentum, we examine the flux of vorticity across the control volume. For steady, two-dimensional Boussinesq flows, the vorticity is governed by

$$\boldsymbol{u} \cdot \nabla \omega = -g' \frac{\partial \rho^*}{\partial x} + \nu \nabla^2 \omega, \tag{2.6}$$

where $\omega = \partial w/\partial x - \partial u/\partial z$ is the vorticity normal to the page and $\rho^* = (\rho - \rho_2)/(\rho_1 - \rho_2)$ denotes the dimensionless Boussinesq density. In deriving (2.6), we have not made the assumption that the flow is hydrostatic. The fact that the pressure does not appear is solely the result of the Boussinesq approximation.

To obtain a control-volume conservation argument, we integrate (2.6) over the entire control volume to produce

$$\oint \omega \boldsymbol{u} \cdot \boldsymbol{n} \, \mathrm{d}S = \iint -g' \frac{\partial \rho^*}{\partial x} \, \mathrm{d}A + \oint \nu \nabla \omega \cdot \boldsymbol{n} \, \mathrm{d}S, \tag{2.7}$$

where $\boldsymbol{n}$ is a unit vector normal to the surface of the control volume. By writing the advective and diffusive terms in (2.7) as surface integrals, we are assuming that the divergence theorem applies.

Both the in- and outflow are normal to the control-volume boundaries, and vorticity is generated only along the interface, i.e. away from the walls. Especially for high-Reynolds-number flows, we can therefore neglect diffusive losses of vorticity across the control-volume boundaries. Equation (2.7) then states that the change in the vorticity flux across the control volume is entirely the result of baroclinic vorticity generation within.

For sharp interfaces, the baroclinic term simplifies to the reduced gravity multiplied by the change in height of the interface: $-g'(h_f - h_a)$ in this case. Upstream of the bore, the velocity field is horizontal and uniform, cf. figure 1(*a*), so no vorticity flows into the control volume. Vorticity exits the control volume as a vortex sheet along the interface between the upper and lower layers, assuming inviscid flow. The vorticity flux carried by a vortex sheet is given as the vortex sheet strength, $\gamma = U_1 - U_2$, multiplied by principal velocity of the sheet, $u_{PV} = (U_2 + U_1)/2$ (Saffman 1992; Pozrikidis 1997). Therefore, (2.7) reduces to

$$\tfrac{1}{2}(U_2^2 - U_1^2) = g'(h_f - h_a). \tag{2.8}$$

Because (2.8) does not contain the pressure, we no longer require a fourth equation relating the energy up- and downstream of the front. Combining (2.8) with the conservation of mass stated in (2.1) and (2.2) produces a closed-form solution for the front velocity of the bore

$$u_{vs} = \left\{ \frac{2R^2(Rr-1)^2}{R - 2Rr + 1} \right\}^{1/2}, \tag{2.9}$$

which we hereafter refer to as the vortex sheet (VS) model.

The evolution of vorticity, as stated in (2.6), can be derived from a linear combination of the conservation equations for both streamwise and vertical momentum. In this way, the streamwise momentum equation does enter into the VS front velocity computation. If we desired, we could now use the conservation of streamwise momentum alone to solve for the pressure jump at the top of the channel given the VS front velocity.

It is also interesting to note that the front velocity in (2.9) can be arrived at by an alternative method. Instead of considering the conservation of circulation, we write the Boussinesq, two-layer shallow-water momentum equations and take their difference to eliminate the pressure at the top of the channel. By considering this equation along with the conservation of mass in (2.1) and (2.2), a shock-joining solution identical to (2.9) can be found (Baines 1995). Sandstrom & Quon (1993) also claim to derive a bore front velocity based on two-layer shallow-water equations for mass

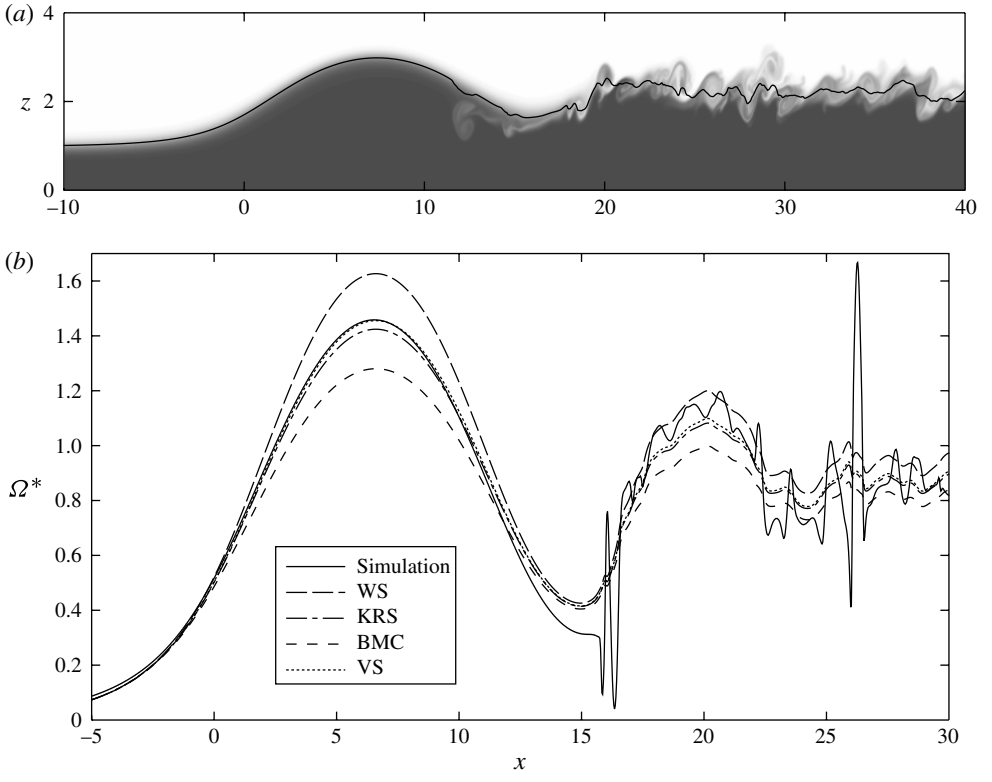

FIGURE 2. (*a*) Density field of a bore from DNS at time $t = 32$ with $R = 2.22$, $r = 0.1$, $Re = 3500$ and $Sc = 1$. (*b*) Measured and predicted vorticity flux as functions of streamwise position. The solid line corresponds to the measured vorticity flux from a DNS with $R = 1.87$, $r = 0.1$, $Re = 3500$ and $Sc = 1$. The dashed lines represent the vorticity flux predicted by the different analytical models. Here, $x = 0$ corresponds to the front of the bore.

and vorticity, but they have not written down their expression for the front velocity, so a comparison with VS cannot be made. Any approach that involves shallow-water equations, however, must assume that the flow near the bore front is hydrostatic in order for the shallow-water equations to apply. Our analysis, on the other hand, does not require such an assumption.

To assess the validity of (2.8) as a jump condition, we can compare its predicted vorticity flux with the actual flux of vorticity in DNS of internal bores using the code of Borden *et al.* (2012). The density field of a representative bore generated by this code is shown in figure 2(*a*). For each analytical model, we compute the predicted vorticity flux $\Omega^* = \int \omega u \, \mathrm{d}z = (U_2^2 - U_1^2)/2g'h_a$ (where $\Omega^* = \Omega/(g'h_a)$ is the dimensionless vorticity flux) as a function of the streamwise position given the local height $h(x) = \int_0^H \rho^*(x, z) \, \mathrm{d}z$.

By comparing these predictions with the actual vorticity flux measured from a DNS (figure 2*b*), we observe that in the quasi-steady region close to the front of the bore, the VS model predicts the correct vorticity flux more accurately than any of the earlier models. In the wake region of the bore, local time-dependent oscillations near the interface degrade the comparison, but spatially averaging the measured vorticity flux in this region in many simulations, each one with a different value of R, reveals that

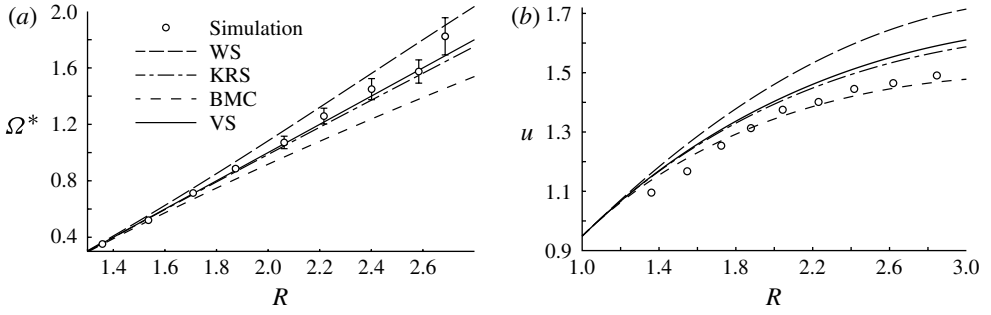

FIGURE 3. (*a*) Averaged vorticity flux in the wake region of internal bores computed for nine values of R with $r = 0.1$, $Re = 3500$ and $Sc = 1$ (circles). The error bars represent a 95 % confidence interval of the mean value. The lines represent the predictions of each model. (*b*) Comparison of the front velocity given by (2.9) with WS, KRS, BMC and DNS data for $r = 0.1$, $Re = 3500$, $Sc = 1$.

the VS model is more accurate than WS and BM (figure 3*a*). Measurement uncertainty clouds any distinction between VS and KRS.

Figure 3(*b*) shows how closely each of the models presented above predicts the front velocity of DNS internal bores as a function of R for $r = 0.1$, $Re = 3500$, and $Sc = 1$. Even though it does the best job of reproducing the correct vorticity flux, the VS model is not as accurate as the KRS and BMC models when it comes to predicting the front velocity. In § 2.3, we explore the reasons for this discrepancy. First however, we consider the energetics of an internal bore, and the implications of the VS model in this context.

2.2. *Energetics*

The models of WS, KRS and BMC all required a condition relating the downstream flux of energy to the upstream flux in order to obtain a closed-form solution for the front velocity of an internal bore as a function of R and r (and Re and Sc for BMC). WS assumes that there is no change in energy flux across the upper layer of a bore, KRS assumes that there is no change in energy flux across the lower layer of a bore, and BMC assumes that there is a slight increase in the energy flux across the lower layer. In contrast, the vortex sheet model makes no assumption about energy conservation across the front of a bore. Therefore, we can now truly predict the energy loss across each layer.

Li & Cummins (1998) developed expressions for the loss of energy in each layer given u, R and r, assuming that the velocity in each layer is uniform and that the downstream interface between the layers is infinitely thin. Substituting the front velocity of the VS model into their relations produces expressions for the change in energy flux across the lower and upper layers, non-dimensionalized by $\dot{e} = \dot{E}/(\rho_1 g'^{3/2} h_a^{5/2})$. The expressions for the change in energy for WS, KRS and BMC are reported in Borden *et al.* (2012).

Table 1 shows the change in energy flux across a bore, separately for each layer and overall, predicted by each model above for a bore with $R = 2$, $r = 0.1$, $Re = 3500$ and $Sc = 1$. All four models predict a global loss of energy across a bore, with the BMC model predicting the largest loss and WS the smallest. The WS and KRS models predict an energy loss entirely confined to one layer and the BMC model predicts that the lower layer gains energy across the front of a bore, as explained in

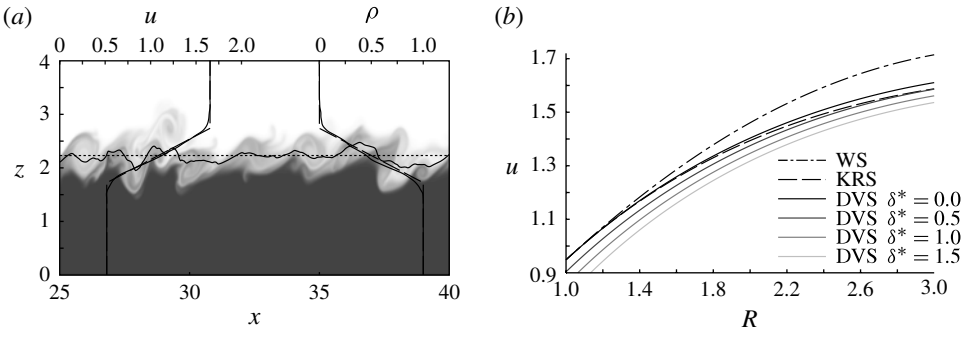

FIGURE 4. (*a*) Density field in the wake region of a DNS internal bore with $r = 0.1$, $R = 2.22$, $Re = 3500$ and $Sc = 1$. The mainly horizontal solid and dashed lines represent the local and average height, respectively, in the wake region. The streamwise-averaged velocity and density profiles are shown with solid lines, and the idealized profiles, which assume a linear profile in the shear layer, are shown with dashed lines. (*b*) Front velocity given by (2.14) plotted for four different values of δ^* (increasing downward). Also shown are KRS and WS for comparison. Here, $r = 0.1$.

Model	$\dot{e}_l$	$\dot{e}_u$	$\dot{e}_t$
WS	−0.122	0	−0.122
KRS	0	−0.168	−0.168
BMC	0.080	−0.278	−0.198
VS	−0.016	−0.146	−0.162

TABLE 1. Energy change in the lower, upper, and both layers predicted by each model for a bore with $R = 2$, $r = 0.1$, $Re = 3500$ and $Sc = 1$.

Borden *et al.* (2012). In their paper, Li & Cummins (1998) show that for internal bores with a discontinuous downstream interface, front velocities faster than WS imply a gain of energy across the upper layer, and velocities slower than KRS imply a gain of energy across the lower layer. It is not surprising, therefore, that the VS model predicts the energy loss is split between each layer, as its front velocity is between WS and KRS.

2.3. *Circulation-based model with diffuse interface*

Each of the above analytical models for internal bores assumes that the interface between the upper and lower layers downstream of the front is infinitely thin, that is, the velocity and density fields are discontinuous across the interface. But if we examine the downstream interface of a simulated bore, as in figure 4(*a*), we see that the average velocity and density profiles transition smoothly over some distance δ between their respective upper- and lower-layer values. In many cases, the value of δ is comparable to h_a, so that including the effects of this mixing layer could have a significant impact on the predicted front velocity.

To account for the effects of this diffuse interface in our vorticity-based model, we assume that the velocity and density vary linearly over the mixing region of thickness δ, which is centred around $z = h_f$ (figure 4*a* shows that this assumption is reasonable). If we define a new coordinate z^*, such that $z^* = 0$ corresponds to the bottom of the

shear layer, then the velocity and density over the interfacial region can be written as

$$u(z^*) = U_1 + \frac{z^*}{\delta}(U_2 - U_1), \tag{2.10}$$

$$\rho^*(z^*) = 1 - \frac{z^*}{\delta}. \tag{2.11}$$

With the diffuse interface, the conservation of mass across each layer can no longer be written as in (2.1)–(2.2). They must now be expressed as

$$\begin{aligned} Uh_a &= U_1\left(h_f - \frac{\delta}{2}\right) + \int_0^\delta u(z^*)\rho^*(z^*)\,\mathrm{d}z^* \\ &= U_1 h_f + \tfrac{1}{6}\delta(U_2 - U_1) \end{aligned}, \tag{2.12}$$

$$\begin{aligned} U(H - h_a) &= U_2\left(H - h_f - \frac{\delta}{2}\right) + \int_0^\delta u(z^*)\left[1 - \rho^*(z^*)\right]\,\mathrm{d}z^* \\ &= U_2(H - h_f) - \tfrac{1}{6}\delta(U_2 - U_1). \end{aligned} \tag{2.13}$$

An expression governing the flux of vorticity can be calculated directly from (2.7) using the velocity and density profiles in (2.10) and (2.11), but the end result is the same as the one given in (2.8). The mixing layer therefore affects the bore velocity only through the conservation of mass, not through the conservation of momentum. Combining (2.12), (2.13) and (2.8) produces the front velocity

$$u_{dvs} = \frac{(R^2 r - R + \delta^*/6)[-6(6Rr - 3R - 3 + \delta^*)]^{1/2}}{6Rr - 3R - 3 + \delta^*}, \tag{2.14}$$

where $\delta^* = \delta/h_a$. Hereafter, we refer to this as the diffuse vortex sheet (DVS) model.

Compared to the WS, KRS and VS models, the DVS model contains an additional unknown, the mixing layer thickness δ^*. Figure 4(*b*) shows that for $\delta^* = 0$, the DVS model collapses to the regular VS model. As δ^* increases, the predicted front velocity decreases uniformly for all values of R.

In order to determine the shear layer thickness δ^* in the DNS, we evaluate the streamwise-averaged velocity and density profiles downstream of the bore, as shown in figure 4(*a*). From the respective endpoints of the velocity profile and its maximum slope, we can then calculate a nominal mixing layer thickness. The resulting values, shown in figure 5(*a*) as a function of R, can be closely approximated by an exponential fit in order to obtain δ^*. Substituting these δ^*-values into (2.14), we find that the DVS model accurately predicts the front velocity of our simulated bores (figure 5(*b*)). This leads us to believe that the only shortcoming of the zero-thickness VS model is its inability to account for mixing in the wake.

Unfortunately, it is not straightforward to develop an analytical expression for δ^* as a function of R and r. In his study on stratified shear layers, Turner (1986) argued that the shear layer thickness grows in the downstream direction until the global decrease in kinetic energy equals the global increase in potential energy (i.e. δ^* tends to the value where $\dot{e}_t = 0$). Using this analysis, he arrived at the relation $\delta = 2\rho_0(\Delta U)^2/g\Delta\rho$. We could follow a similar approach, where we compute $\dot{e}_t$ as a function of δ^* for a DVS internal bore, and choose the value of δ^* where $\dot{e}_t$ is zero.

To compute the change in energy flux for the DVS model, we cannot use Li & Cummins' expressions because we no longer have a thin downstream interface. Instead, we must directly calculate and subtract the upstream flux of energy from the

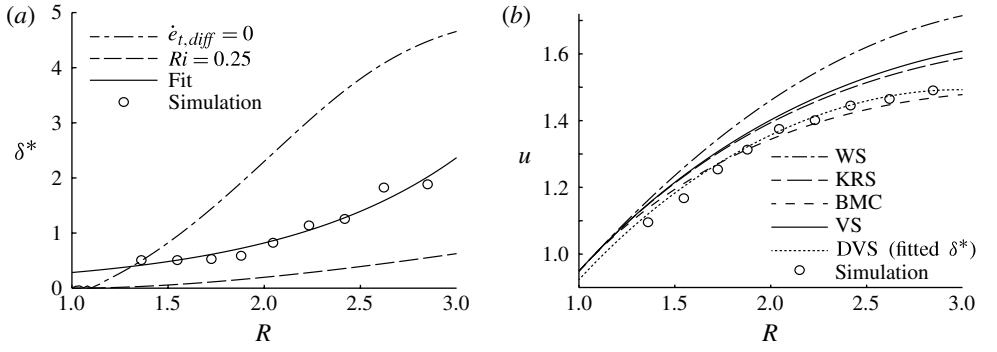

FIGURE 5. (*a*) Dimensionless interface thickness of our simulations (○) plotted as a function of R for $r = 0.1$, $Re = 3500$ and $Sc = 1$. The solid line represents an exponential fit to the data ($\delta^* = 0.09848\exp(1.06R)$). (*b*) Front velocity given by (2.14) where δ^* is given by the exponential curve in (*a*). Also shown are the WS, KRS and VS models for comparison.

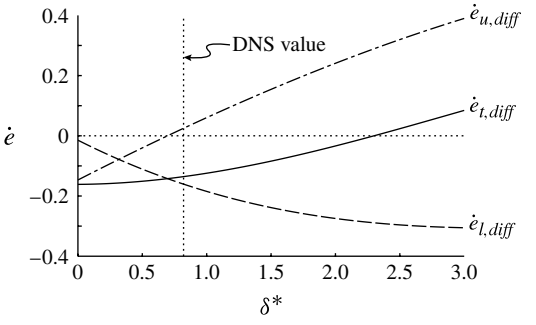

FIGURE 6. Change in energy flux across each layer ($\dot{e}_{l,diff}$ and $\dot{e}_{u,diff}$) and globally ($\dot{e}_{t,diff}$) as a function of the downstream shear layer thickness for $R = 2$ and $r = 0.1$.

downstream flux in each layer with the expression

$$\dot{e}_{diff} = \left[\int_0^{1/r} A(z)u(z)\left(\tfrac{1}{2}u(z)^2 + \rho^*(z)z + p(z)\right)\,\mathrm{d}z\right]_u^d, \tag{2.15}$$

where $A(z) = \rho^*(z)$, $1 - \rho^*(z)$, or 1 depending on whether we wish to isolate the upper or lower layer, or consider both layers together.

Figure 6 shows the change in energy flux in each layer as a function of the downstream shear layer thickness. The mixing that produces the diffuse interface pulls some light, high-speed fluid from the upper layer into the lower layer and pushes some dense, low-speed fluid from the lower layer into the upper layer. The kinetic, potential and pressure energy flux terms are affected oppositely in each layer, but the net effect is an increase in the energy flux of the upper layer, a decrease in the lower layer, and an increase in the total flux compared with the zero-thickness VS model.

For the value of δ^* measured in the DNS, the DVS model predicts a gain in energy across the upper layer of the bore. There is a certain critical value of δ^* above which the energy change in the upper layer is positive, and another critical value above which the total energy change is also positive. These critical values are functions of R and r.

The critical value where $\dot{e}_{t,diff} = 0$ always exists for any realistic value of R and r. It is tempting to analytically solve for δ^* by requiring that a bore conserve energy (i.e. that $\dot{e}_{t,diff} = 0$). However, notice that in both figures 5(*a*) and 6 the value of δ^* where $\dot{e}_{t,diff} = 0$ is significantly greater than the actual value of δ^* measured in the DNS. Turner (1986) noticed this same discrepancy in his research; his energy balance always significantly over-predicted the thickness of his experimental stratified shear layers. He attributed the error to the neglect of viscous losses due to shear and proposed that his energy analysis be used only as a scaling argument, not an equality. Therefore, although setting $\dot{e}_{t,diff} = 0$ provides an upper limit on the shear layer thickness, it does not produce an accurate value and therefore would not provide a meaningful analytical model.

Finally, we attempted to use the linear stability analysis for a stratified shear layer presented in Turner (1973) to determine δ^*. That analysis found that disturbances of all wavenumbers are stable if $Ri \geqslant 0.25$, where $Ri = g'\delta^*/(\Delta u)^2$ is the gradient Richardson number. Unfortunately, figure 5(*a*) shows that this stability criterion underestimates the thickness. We believe the discrepancy is due to diffusion, unaccounted for in the stability analysis but present in our DNS.

3. Conclusions

We have shown that by considering the transport of interfacial vorticity, it is possible to produce an analytical model that describes the propagation of internal bores without resorting to the traditional assumptions of energy conservation used by existing models. Furthermore, we have shown that the biggest shortcoming of this vortex sheet model is its inability to account for mixing produced by shear at the interface downstream of the front of a bore. If it incorporates shear layer thickness data from a DNS, the present model very closely reproduces the DNS bore velocity data. For future work, it would be interesting to extend this analysis to bores propagating into a shear flow. This would involve modifying (2.8) to account for vorticity entering the control volume from upstream. We are also working on extending the VS model to non-Boussinesq flows.

Acknowledgements

This work was supported through NSF grants CBET-0854338, CBET-1067847 and OCE-1061300.

References

Baines, P. G. 1995 *Topographic Effects in Stratified Flows*. Cambridge University Press.

Borden, Z., Meiburg, E. & Constantinescu, G. 2012 Internal bores: an improved model via a detailed analysis of the energy budget. *J. Fluid Mech.* **703**, 279–314.

Clarke, R. H., Smith, R. K. & Reid, D. G. 1981 The morning glory of the gulf of Carpentaria: an atmospheric undular bore. *Mon. Weath. Rev.* **109**, 1726–1750.

Gonzalez-Juez, E., Meiburg, E., Tokyay, T. & Constantinescu, G. 2010 Gravity current flow past a circular cylinder: forces, wall shear stresses and implications for scour. *J. Fluid Mech.* **649**, 69–102.

Haase, S. P. & Smith, R. K. 1984 Morning glory wave clouds in Oklahoma: a case study. *Mon. Weath. Rev.* **112**, 2078–2089.

Klemp, J. B., Rotunno, R. & Skamarock, W. C. 1997 On the propagation of internal bores. *J. Fluid Mech.* **331**, 81–106.

LEICHTER, J. J., WING, S. R., MILLER, S. L. & DENNY, M. W. 1996 Pulsed delivery of subthermocline water to Conch Reef (Florida Keys) by internal tidal bores. *Limnol. Oceanogr.* **41** (7), 1490–1501.

LI, M. & CUMMINS, P. F. 1998 A note on hydraulic theory of internal bores. *Dyn. Atmos. Oceans* **28**, 1–7.

MOROZOV, E. G., TRULSEN, K., VELARDE, M. G. & VLASENKO, V. I. 2002 Internal tides in the straight of Gibraltar. *J. Phys. Ocenaogr.* **32**, 3193–3206.

POZRIKIDIS, C. 1997 *Introduction to Theoretical and Computational Fluid Dynamics*. Oxford University Press.

RAYLEIGH, LORD 1914 On the theory of long waves and bores. *Proc. R. Soc. Lond.* A **90** (619), 324–328.

SAFFMAN, P. G. 1992 *Vortex Dynamics*. Cambridge University Press.

SANDSTROM, H. & QUON, C. 1993 On time-dependent, two-layer flow over topography. I. Hydrostatic approximation. *Fluid Dyn. Res.* **11**, 119–137.

TURNER, J. S. 1973 *Buoyancy Effects in Fluids*. Cambridge University Press.

TURNER, J. S. 1986 Turbulent entrainment: the development of the entrainment assumption, and its application to geophysical flows. *J. Fluid Mech.* **173**, 431–471.

WAKIMOTO, R. M. & KINGSMILL, D. E. 1995 Structure of an atmospheric undular bore generated from colliding boundaries during CaPE. *Mon. Weath. Rev.* **123**, 1374–1393.

WOOD, I. R. & SIMPSON, J. E. 1984 Jumps in layered miscible fluids. *J. Fluid Mech.* **140**, 215–231.